Irreversibility Analysis of an Ejector Refrigeration Cycle by Modified Gouy-Stodola Formulation

Sachdeva, Gulshan
National Institute of Technology Kurukshetra

Sharma, Bharat
National Institute of Technology Kurukshetra

Anuradha, Parinam
U.I.E.T., Kurukshetra University

Verma, Sameer
National Institute of Technology Kurukshetra

https://doi.org/10.5109/6781075

出版情報：Evergreen. 10 (1), pp.252-271, 2023-03. 九州大学グリーンテクノロジー研究教育センター
バージョン：

Irreversibility Analysis of an Ejector Refrigeration Cycle by Modified Gouy-Stodola Formulation

Gulshan Sachdeva[1], Bharat Sharma[1,*], Parinam Anuradha[2], Sameer Verma[1]

[1]National Institute of Technology Kurukshetra, India

[2]U.I.E.T., Kurukshetra University, Kurukshetra, India

*Author to whom correspondence should be addressed:

E-mail: bharat_61900103@nitkkr.ac.in

(Received December 11, 2022; Revised February 9, 2023; accepted February 23, 2023).

Abstract: In this paper, irreversibility analysis of an ejector refrigeration system (ERS) is carried out using modified Gouy-Stodola formulation that incorporates the use of an effective temperature unlike the surrounding temperature employed in classical Gouy-Stodola equation for the irreversibility determination. The components of any system do not transfer heat at surrounding temperature all the times and thus some error is involved in the analysis, as the conventional equation calculates irreversibility using the surrounding temperature. The use of effective temperature provides more accurate measurement of exergy destruction. R1234ze is the refrigerant in this study due to its low Global Warming Potential (GWP) and zero Ozone Depletion Potential (ODP) and is compared with its counterpart R134a. The study is conducted for a fixed 10 kW cooling system. The coefficient of performance (COP) is found to increase by 15.93% and 11.68% for R1234ze and R134a respectively with the change in generator temperature from 91°C to 99°C. However, the drop in COP is 52.38% and 58.54% for R1234ze and R134a respectively with increase in condenser temperature from 32°C to 40°C. It shows that R1234ze performs better than R134a. Due to the highest coefficient of structural bonding (CSB) value in the evaporator, the change in total irreversibility is particularly susceptible to changes in evaporator temperature.

Keywords: Exergy, irreversibility, effective temperature, ejector refrigeration system, coefficient of structural bonds.

1. Introduction

A vapor compression refrigeration system (VCRS) is mostly used in various cooling applications, but it has a significant downside that it requires a large amount of electrical energy to run its compressor. Thus it causes the power plants to burn more and more fossil fuel to generate more electricity and the adverse outcomes are more carbon emissions and greenhouse effect. In contrast, the electricity consumption is negligible in ejector refrigeration system (ERS) wherein an ejector substitutes the mechanical compressor. The ERS needs heat at low temperature that can be supplied managing solar heat systems, geothermal wells, bio-gasifiers etc. at a very low cost. The benefits include cost saving, long life, no moving parts but the pump, and ease of construction. Though vapour absorption system is also a heat driven system but it captures a little market due to its bulky size, high investment cost, and mainly the requirement of heat energy in abundance at high temperature. Keenan et al. [1)] proposed the ejector theory in 1950 that has been serving as the foundation for various ejector models till now. Huang et al. [2)] performed 1-D study assuming constant-pressure mixing model taking R141b working fluid. They validated their numerical model with the experiments conducted with 11 different ejectors and mainly verified the entrainment ratio (μ) of ejector. Selvaraju and Mani [3)] experimented ERS with R134a and concluded that raising the generator temperature improved coefficient of performance (COP), entrainment ratio (μ) and cooling capacity up to a certain extent but degraded thereafter. So there exists a single generator temperature for the specified condenser & evaporator temperatures at which the COP is maximum. Sankarlal and Mani [4)] experimented ERS with ammonia and concluded that increasing the expansion ratio and area ratio improved μ and COP. The expansion ratio is the ratio of generator to evaporator pressures. Chen et al. [5)] evaluated optimum performance and ejector area ratio of ERS. They concluded that increase in evaporator and generator temperatures do improve the entrainment ratio but the rise in condenser temperature drops the entrainment ratio. A compressor, a gas cooler, and one turboexpander are added between the secondary inlet flow of the ejector and the evaporator in Purjam et. al. [6)] simulation of the modified ejector refrigeration cycle. The modified system obtained the

maximum COP 1.342 at fixed sink and source temperature 303K and 233K respectively. Yan et al. [7] worked experimentally on an R134a ejector refrigeration system and found that when back pressure was less than critical back pressure, the ejector worked at the optimum performance. The ejector managed to operate in single choking mode till the critical back pressure. They also concluded that the critical back pressure got improved with the rise in motive fluid pressure but fixed secondary fluid pressure; however, it decreased the maximum entrainment ratio. Kumar and Sachdeva[8,9] performed experiments with different size of ejectors at same designed conditions and predicted that the system performed better at the optimum ejector area ratio. Researchers[10,11] used steam and R123 in an experimental analysis of the ejector cooling system under various operating conditions, and they found COP between 0.17 and 0.5. Similar experiment was conducted by Sag and Ersoy [12]. They investigated the effect of external fluid temperature of condenser and found the COP improvement from 5.1 to 12.6% at 2.3mm throat diameter. Kitrattana[13] analysed one-dimensional ejector model considering real fluid properties and further compared with Keenan et al. [1] model. Sharma et al. [14] obtained COP of ECS between 0.13-0.33 at the generator temperature 90°C while varying condenser and evaporator temperatures in the range of 33-35°C and 0-4°C, respectively using R1234yf as refrigerant.

George Andrian Untea et al. [15] performed 1st and 2nd law analyses of ERS with water, methanol, NH_3, and R134a and obtained 0.48 as the maximum COP with water. Operating the system at generator 140°C, condenser 30°C and evaporator 5°C provided 8.5% exergetic efficiency. The maximum 2nd law efficiency was found to be 53.32% with R134a at condenser 30°C and evaporator 5°C. Exergy evaluations of ERS using various refrigerants were done by Baruah et al. [16]. Pridasawas et al. [17] executed exergy analysis of the ERS with butane and found the maximum irreversibility in ejector. Paridasawas findings were later verified by Alexis [18] who worked with water as a refrigerant. The results obtained by Dahmani et al. [19] manifested that a major portion of the availability destruction occurred in ejector with R134a refrigerant. The exergy analyses done by these researchers were based on the conventional Gouy-Stodola equation. Chen et al. [20] conducted advanced exergy analysis of ERS. The analysis divided the exergy loss into endogenous and exogenous components. They observed that 35% of the total exergy loss could be prevented. Chen et al. [21] evaluated the ERS with five environment friendly refrigerants R600, R600a, R601a, R1233zd(E) and R1234ze(E).

Researchers[22,23] have also examined transcritical ejector cycles with CO_2 as a working fluid. It is a cycle in which working fluid passes through both sub-critical and supercritical states. Deng et al. [24] investigated a transcritical CO_2 cooling cycle employing an ejector and concluded that relative to the standard cycle, an ejector reduced 23% of the total exergy destruction. Yari M[25] obtained 12.5–21% higher COP with a transcritical CO_2 refrigeration cycle in comparison to a conventional 2-stage refrigeration system. Liu et al. [26] carried out conventional and advanced exergy analyses of transcritical CO_2 ERS coupled with subcooler. It reduced the exergy destruction from 89.44% to 56.36% by improving the components. Daqing et al. [27] and Goa et al. [28] also obtained COP improvement of 16% and 29% with the ejector-expansion cycle as compared to the conventional cycle. Many researcher[29,30] was performed experiments obtained that COP increased from 3-7% compare to basic ERS cycle.

The analyses of ERS on the basis of energy conservation have been carried out by many researchers either with the natural refrigerants or sub-critical refrigerants but having high ODP and GWP which are going to be discontinued soon. The ejector refrigeration system needs to be evaluated with the new refrigerants having environment friendly properties. The refrigerant R1234ze considered in this study is amongst those refrigerants. Moreover, the irreversibility determined by the conventional Gouy-Stodola equation may conclude some wrong observations about the components of a system. This study focuses on the modified Gouy-Stodola formulation which is more realistic and accurate.

To determine system loss and potential of improvement, exergy analysis is crucial[31]. In practice, all thermodynamic processes are irreversible and the irreversible loss is computed using conventional Gouy-Stodola theorem:

$$\dot{I} = T_0 \dot{S}_{gen} \quad (1)$$

where T_0 represents surrounding temperature in K and $\dot{S}_{gen}$ represents rate of entropy generation in kJ/kg-K during the process.

Eq. 1 is valid if a system exchanges heat with the surroundings only. However, if the systems transfer heat at temperature different than the surrounding temperature, Eq. 1 does not give the realistic values of irreversibility [32] . Holmberg et al. [32] found contradictive results in an industrial process of a CHP plant. They found that the actual power loss in the process is greater in winter than the summer when it was calculated by the modified method, however, the power was found to be higher in summer when calculated by the conventional Gouy-Stodola equation. Lampinen and Wiksten[33] used effective temperature in Eq. 1, instead of surrounding temperature to obtain more realistic results. Perera et. al. [34] developed an experimental setup for cooling based on vapor compression system and predicted the highest exergy destruction in compressor with R410a as working fluid. Vaibhav et al. [35,36] performed exergy investigation of a cascaded vapor compression–absorption cooling cycle considering modified formulation. Sachdeva and Sharma[37,38] did the exergy analysis of an ERS based on conventional and modified Gouy-Stodala equation and

predicted that ejector showed highest irreversibility at the designed conditions.

Lampinen and Wiksten[33] proposed modification in the Gouy-Stodola equation as under:

$$W_{max} - W = T_{eff}\dot{S}_{gen} \quad (2)$$

where W_{max} is the maximum work in kW; W is the actual work in kW; and T_{eff} is the effective temperature in K.

The energy balance for a fluid flow is given by:

$$W = \dot{m}(h_1 - h_2) + Q \quad (3)$$

where W is the actual work in kW; h_1 & h_2 represent specific enthalpies at inlet and outlet respectively in kJ/kg; and Q is the net heat supplied to the cycle in kW.

From the second law of thermodynamics

$$\dot{m}(s_2 - s_1) = \int_1^2 \frac{dQ}{T} + \dot{S}_{gen} \quad (4)$$

where s_1 and s_2 represent specific entropies at inlet and outlet respectively in kJ/kg-K; and T is the boundary temperature in K.

In a reversible process, there is no entropy generation, thus-

$$W_{max} = \dot{m}(h_1 - h_{2r}) + Q \quad (5)$$

$$\dot{m}(s_{2r} - s_1) = \int_1^2 \frac{dQ}{T} \quad (6)$$

where h_{2r} and s_{2r} are enthalpy and entropy respectively after a reversible process.

Lampinen and Wiksten[33] provided the integral of $\int_1^2 \frac{dQ}{T}$ as under

$$\frac{Q}{T_{eff}} = \int_1^2 \frac{dQ}{T} \quad (7)$$

By subtracting Eq. 3 from Eq. 5 and on further solving

$$W_{max} - W = \dot{m}(h_2 - h_{2r}) \quad (8)$$

Substitute Eq. 6 in Eq. 4 and on solving

$$\dot{S}_{gen} = \dot{m}(s_2 - s_{2r}) \quad (9)$$

Substituting Eq. 8 and 9 in Eq. 2, the effective temperature formulation is as under [32].

$$T_{eff} = \frac{h_2 - h_{2r}}{s_2 - s_{2r}} \quad (10)$$

The effective temperature (T_{eff}) formulation can be presented in terms of temperatures for the ideal gases[32].

$$T_{eff} = \frac{T_2 - T_{2r}}{\ln\frac{T_2}{T_{2r}}} \quad (11)$$

where T_{2r} represents outlet temperature considering the process to be reversible and T_2 is the actual outlet temperature in K.

In this paper, the modified approach is used to calculate irreversibility in each component of the ERS and the outcomes are compared with those found by the conventional equation. The working fluids are R1234ze and R134a. The irreversibility of the components varies with the operating parameters and the change in total irreversibility of system due to the change in irreversibility of one component is better understood by the coefficient of structural bonds (CSB). It has been presented in a lucid manner in the present study. The CSB analysis finds the component whose operating variables make the system the most irreversible.

2. System description

The ERS consists of generator, ejector, condenser, evaporator, throttling device and pump as depicted in Fig. 1-a. The ejector somehow plays the role of a compressor in the system. It mainly comprises four geometrical sections i.e. convergent-divergent primary/motive nozzle, suction section, constant area segment (CAS) and diffuser. The vapor refrigerant exiting the generator at high pressure is called the primary fluid. It expands in the primary nozzle and thus pressure becomes lower at its exit than the pressure in evaporator. Consequently, the ejector sucks vapor exiting from the evaporator which is called the secondary fluid. After mixing of these fluid streams, the velocity of flow is still supersonic in the mixing section and gets reduced to subsonic because of the normal shock generation before entering to the diffuser section. The subsonic diffuser increases pressure of the refrigerant up to the condenser pressure. A part of the condensed liquid refrigerant goes into the evaporator through a throttling valve and there takes the cooling load. The other part is pumped to the generator and this way completes the cycle.

In Fig. 1-b, process 1-e_1 represents expansion of primary fluid in the nozzle at constant entropy and e_1' represents the state point after considering isentropic efficiency of the nozzle. The process 6-e_2 is the isentropic expansion of secondary fluid. The state point e_3 represents the state of mixed fluid and e_4 is the state of shock wave. The pressure recovery in the diffuser is shown by the process e_4-2. The state 2´represents the state taking diffuser efficiency into account. The process 2-3 happens in the condenser and the pump raises pressure of the condensed refrigerant up to the generator pressure i.e. state point 4. The generator supplies heat to the refrigerant and transforms it into saturated vapor as per the state point 1 and completes the primary cycle. The remaining part of the liquid at point 3 expands irreversibly in expansion device up to state 5 and provides cooling in the evaporator. At the exit of evaporator, the working fluid is saturated vapor and these vapor are sucked by the ejector and this way completes the secondary cycle.

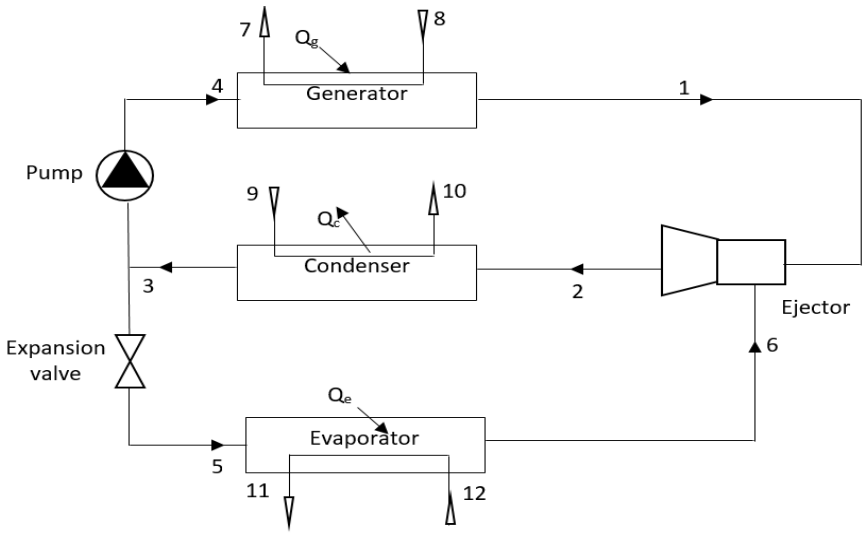

Fig. 1-a: Ejector Refrigeration System

3. Thermodynamic modeling and assumptions

The below mentioned assumptions are considered to ease the analysis:

I. Steady state conditions prevail at all the state points.
II. Pressure drop and heat losses are negligible in heat exchangers and tubes.
III. The velocity of primary and secondary flow at the inlet of ejector is negligible.
IV. The velocity of the mixed flow coming out of the ejector is also neglected.
V. The working fluid is saturated at the exit of generator, condenser, and evaporator.

Thermodynamic modelling includes mass, energy and entropy balance as shown below.

i. Mass conservation $\sum \dot{m}_{out} = \sum \dot{m}_{in}$
ii. Energy conservation $\sum Q_{out} + \sum \dot{W}_{out} + \sum \dot{m}_{out} h_{out} = \sum Q_{in} + \sum \dot{W}_{in} + \sum \dot{m}_{in} h_{in}$
iii. Entropy generation $\sum \dot{m} s_{out} = \sum \dot{m} s_{in} + \sum \dot{Q}/T + \dot{S}_{gen}$

Table 1 provides the formulations to get effective temperature of all the components. The subscripts used in these equations are as per the state points depicted in figure 1-a.

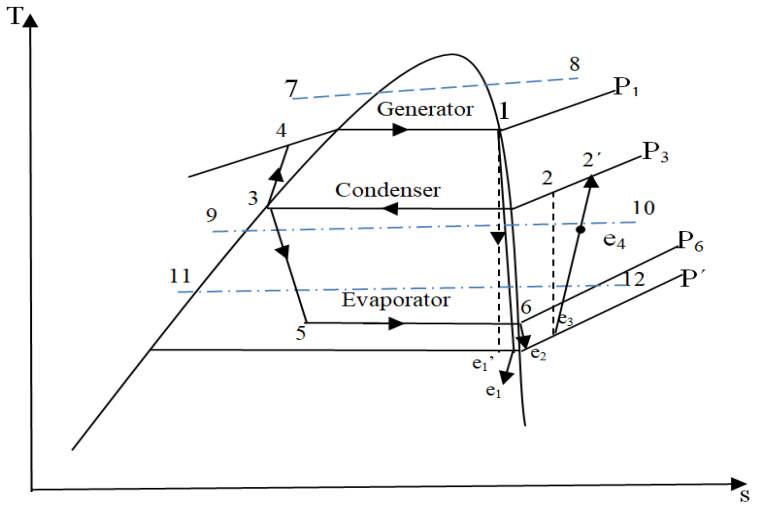

Fig. 1-b: T-s diagram of the ERS

Table 1: Effective temperature formulations

S. No	Component	Effective Temperature Formulation
1	Evaporator	$\dot{S}_{gen,Eva} = \dot{m}_6(s_6 - s_5) + \dot{m}_{11}c_p \ln \frac{T_{11}}{T_{12}}$ $0 = \dot{m}_6(s_6 - s_5) + \dot{m}_{11}c_p \ln \frac{T_{11r}}{T_{12}}$ $T_{eff,Eva} = \frac{T_{11} - T_{11r}}{\ln \frac{T_{11}}{T_{11r}}}$
2	Condenser	$\dot{S}_{gen,Con} = \dot{m}_2(s_3 - s_2) + \dot{m}_{10}c_p \ln \frac{T_{10}}{T_9}$ $0 = \dot{m}_2(s_3 - s_2) + \dot{m}_{11}c_p \ln \frac{T_{10r}}{T_9}$ $T_{eff,Con} = \frac{T_{10} - T_{10r}}{\ln \frac{T_{10}}{T_{10r}}}$
3	Generator	$\dot{S}_{gen,Gen} = \dot{m}_1(s_1 - s_4) + \dot{m}_7c_p \ln \frac{T_7}{T_8}$ $0 = \dot{m}_1(s_1 - s_4) + \dot{m}_7c_p \ln \frac{T_{7r}}{T_8}$ $T_{eff,Gen} = \frac{T_7 - T_{7r}}{\ln \frac{T_7}{T_{7r}}}$
4	Pump	$\dot{S}_{gen,Pump} = \dot{m}_1(s_4 - s_3)$ $T_{4r} = T_4$ $T_{eff,Pump} = T_{4r}$
5	Ejector	$T_{2r} = T_2$ $T_{eff,Eje} = T_{2r}$
6	Throttling Valve	$T_{5r} = T_5$ $T_{eff,TV} = T_{5r}$

The exergy destruction of the system and its components has been related to the structural coefficients. If a small increase in the irreversibility rate of one component caused by the change in its operating temperature, results in a significant change in overall irreversibility of the cycle; it is preferred to put more efforts in designing that component. The CSB value is high for such components. Thus much focus must be made to enhance the performance of components having high CSB values. Nikolaidis and Probert[39] and Gebreslassie et al. [40] defined CSB as Eq. 12.

$$\sigma_k = [\frac{\partial \dot{I}_t}{\partial x_i}]/[\frac{\partial \dot{I}_k}{\partial x_i}] \quad (12)$$

Here $\dot{I}_k$ is the irreversibility rate of k^{th} component and x_i is the variable that is varied in the component k.

3.1 Governing equations:

Thermodynamic equations used for the ejector are given below. Ideal gas behavior is assumed and subscripts used in these equations are according to the figure shown in 1-b.

3.1.1 Primary/Motive flow 1-e_1:

Velocity of the primary fluid at the nozzle exit (u_{e1}) is given by equations 13 and 14:

$$u_{e1} = \sqrt{2\eta_n(h_1 - h_{e1'})} \quad (13)$$

$$h_{e1'} = f(P', s_1) \quad (14)$$

where P′ is the mixing pressure in the ejector.
Isentropic efficiency of the nozzle is calculated by equation 15:

$$\eta_n = \frac{h_1 - h_{e1}}{h_1 - h_{e1'}} \quad (15)$$

Mach number of the primary/motive flow at the nozzle outlet is managed by equation 16:

$$Ma_{PF,e1} = \left[\frac{2\eta_n\left[\left(\frac{P_1}{P'}\right)^{\frac{k-1}{k}} - 1\right]}{k-1}\right]^{1/2} \quad (16)$$

3.1.2 Secondary flow 6-e_2:

The actual mixing pressure should be lower than the secondary pressure; however to simply the model, many researchers[17,41] assumed the mixing pressure same as the secondary pressure. In the present analysis, mixing pressure is considered same as the exit pressure of primary fluid and it is lower than the evaporator pressure. The velocity of the secondary fluid at e_2 is given by equation 17 and 18:

$$u_{e2} = \sqrt{2\eta_n(h_6 - h_{e2})} \quad (17)$$

$$h_{e2} = f(P', s_6) \quad (18)$$

Mach number of secondary fluid at e_1 is given by [42] equation 19:

$$Ma_{SF,e1} = \left[\frac{2\left[\left(\frac{P_6}{P'}\right)^{\frac{k-1}{k}} - 1\right]}{k-1}\right]^{1/2} \quad (19)$$

3.1.3 Mixing process before shock (e_1 & e_2 to e_3):

Momentum balance as shown in equation 20 to get the mixing velocity:

$$u_{e3} = \frac{u_{e1} + \mu' u_0}{1+\mu'} \quad (20)$$

where μ′ is an assumed entrainment ratio of the ejector, defined as the ratio of the secondary mass flow rate to the primary mass flow rate.

The mixing efficiency η_m is stated in equation 21:

$$\eta_m = \frac{u_{e3}^2}{u_{e3'}^2} \quad (21)$$

The velocity and enthalpy of real mixing process (u_{e3}, h_{e3}) are given by equations 22 to 24[41]:

$$u_{e3} = u_{e3'}(\eta_m)^{1/2} = \frac{u_{e1} + \mu' u_0}{1+\mu'}(\eta_m)^{1/2} \quad (22)$$

$$h_{e3} = \frac{h_1 + \mu' h_6}{1+\mu'} - \frac{u_{e3}^2}{2} \quad (23)$$

$$s_{e3} = f(P', h_{e3}) \quad (24)$$

The correlation between Critical Mach number Ma^* and Mach number of motive and secondary fluid respectively is given by equations 25 and 26:

$$Ma^*_{PF,e1} = \left(\frac{Ma^2_{Gen,e1}(k+1)}{Ma^2_{Gen,e1}(k-1)+2}\right)^{1/2} \text{ and}$$

$$Ma^*_{SF,e1} = \left(\frac{Ma^2_{Eva,e1}(k+1)}{Ma^2_{Eva,e1}(k-1)+2}\right)^{1/2} \quad (25)$$

The Critical Mach number at e_3 considering mixing efficiency (η_m) is managed in equation 26:

$$Ma^*_{e3} = \eta_m^{1/2} \frac{\left(Ma^*_{PF,e1} + \mu' Ma^*_{SF,e1}\left(\frac{T_{Eva}}{T_{Gen}}\right)^{1/2}\right)}{\sqrt{(1+\mu')\left(1+\mu'\frac{T_{Eva}}{T_{Gen}}\right)}} \quad (26)$$

The Mach number at state e_3 is given by equation 27:

$$Ma_{e3} = \left(\frac{2Ma^{*\,2}_{e3}}{(k+1) - Ma^{*\,2}_{e3}(k-1)}\right)^{1/2} \quad (27)$$

3.1.4 Flow in the diffuser e_3-2:

Since the velocity at the outlet of diffuser is not considered, therefore enthalpy at the exit of diffuser (h_2) is given as:

$$h_2 = h_{e3} + \frac{u_{e3}^2}{2} \quad (28)$$

$$h_2 = h_{e3} + \frac{h_{2'} - h_{e3}}{\eta_d} \quad (29)$$

$$h_{2'} = f(P_{Con}, s_{e3}) \quad (30)$$

where $h_{2'}$ is the isentropically exit enthalpy of diffuser at condenser pressure.

Diffuser efficiency η_d is given by equation 31:

$$\eta_d = \frac{h_{2'} - h_{e3}}{h_2 - h_{e3}} \quad (31)$$

Entrainment ratio is obtained by managing equations 13, 17, 28 and 31, that turns into equation 32

$$\mu = \frac{\sqrt{2\eta_n(h_1 - h_{e1})} - \sqrt{2(h_{2'} - h_{e3})/(\eta_d\eta_m)}}{\sqrt{2(h_{2'} - h_{e3})/(\eta_d\eta_m)} - \sqrt{2(h_6 - h_{e2})}} \quad (32)$$

Due to shock formation pressure increases and velocity decreases. Mach number and pressure at state e_5 are written as equations 33 and 34 considering ideal gas behavior[43]:

$$\mathrm{Ma}_{e4} = \left(\frac{\mathrm{Ma}_{e_3}^2 + 2/(k-1)}{2k\mathrm{Ma}_{e_3}^2/(k-1) - 1}\right)^{1/2} \quad (33)$$

$$\frac{P_{e4}}{P_{e3}} = \frac{1+k\mathrm{Ma}_{e3}^2}{1+k\mathrm{Ma}_{e4}^2} \quad (34)$$

Pressure recovery in the diffuser (e_4-2) is given by equation 35[43]:

$$\frac{P'_{Con}}{P_{e4}} = \left[\frac{(k-1)}{2}\mathrm{Ma}_{e4}^2 + 1\right]^{k/(k-1)} \quad (35)$$

where P'_{Con} is the calculated ejector outlet pressure which is to be iterated to get the pressure equal to the condenser pressure.

3.1.5 Area ratio and COP:

The area ratio (AR) is stated as the ratio of area of constant area section to the primary nozzle throat area and it can be obtained using equation 36.

$$\mathrm{AR} = \frac{\text{Area of constant area section}}{\text{nozzle throat area}}$$

$$AR = \frac{P_{Gen}\sqrt{(1+\mu)}\sqrt{1+\mu\frac{T_{Eva}}{T_{Gen}}}\left(\frac{2}{k+1}\right)^{\frac{1}{k-1}}\sqrt{1-\frac{2}{k+1}}}{P_{Con}\left(\frac{P_{e4}}{P_{Con}}\right)^{\frac{1}{k}}\sqrt{1-\left(\frac{P_{e4}}{P_{Con}}\right)^{\frac{k-1}{k}}}} \quad (36)$$

The entrainment ratio and COP of the cycle are found using equations 37 and 38 as under:

$$\text{Entrainment Ratio}, \mu = \frac{\dot{m}_{Eva}}{\dot{m}_{Gen}} \quad (37)$$

$$\mathrm{COP} = \frac{\text{refrigerating effect produced in the evaporator}}{\text{heat added in the generator}} =$$

$$\mu\frac{h_6 - h_5}{h_1 - h_3} \quad (38)$$

3.2 Computational procedure:

Fig. 2 shows computational procedure adopted to analyze the system.

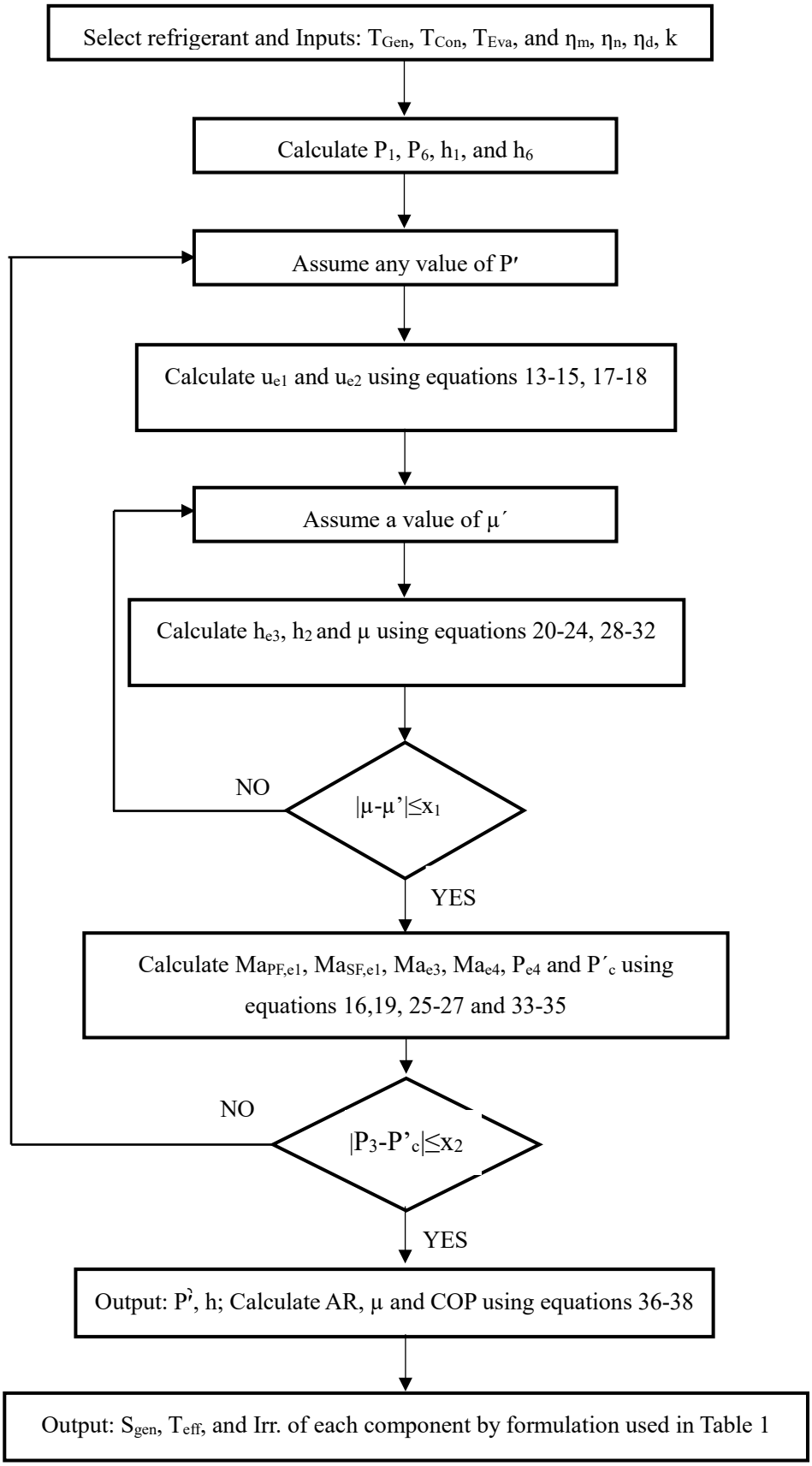

Fig. 2: Flow chart

3.3 Model Validation

The performance parameters i.e. COP, Area Ratio and Entrainment Ratio obtained using the current model have been validated with Saleh B. [44] for the refrigerant R134a. Table 2 shows that the variation of these parameters with respect to generator temperature are in coherence with the work[44]. The exergy destruction and exergetic efficiency of the components of ERS using conventional Gouy-Stodola equation are also compared with the same determined by Chen et al. [20] for R245fa refrigerant. The exergy of the fuel and product[45] are evaluated at generator, condenser and evaporator temperatures of 95°C, 35°C and 8°C respectively. Exergy loss is the difference between the exergy of fuel and product. The ratio of the exergy of product and fuel is called exergetic efficiency. The current numerical analysis has been executed using Engineering Equation Solver (EES) [46]. Table 3 shows that exergy destruction and exergetic efficiency of the components are almost same as obtained by Chen et al. [20] and thus validates the current model.

Table 2. Comparison of results with Saleh B. [44]

	Saleh B. [44]			Current Model		
T_{Gen} (°C)	COP	μ	AR	COP	μ	AR
70	0.06	0.073	2.96	0.075	0.083	2.44
75	0.109	0.126	3.39	0.115	0.13	3.89
80	0.15	0.173	3.87	0.159	0.185	4.24
85	0.185	0.213	4.39	0.189	0.213	4.79
90	0.215	0.243	4.95	0.214	0.239	5.02
95	0.235	0.259	5.56	0.227	0.266	6.02
100	0.239	0.301	6.57	0.243	0.293	6.59

Table 3. Comparison of results with Chen et al. [20]

	Chen et al. [20]				Current Model			
Components	$\dot{E}_F$ (kW)	$\dot{E}_P$ (kW)	$\dot{E}_D$ (kW)	ε %	$\dot{E}_F$ (kW)	$\dot{E}_P$ (kW)	$\dot{E}_D$ (kW)	ε%
Generator	6.180	4.879	1.301	78.9	6.238	4.92	1.318	78.8
Condenser	1.429	0.591	0.838	41.3	1.456	0.618	0.836	42.5
Evaporator	0.604	0.437	0.167	72.4	0.599	0.4324	0.167	72.0
Ejector	3.993	1.166	2.827	29.2	4.013	1.165	2.848	29.0
Pump	0.123	0.093	0.03	75.6	0.125	0.094	0.03	75.0
Throttling valve	0.742	0.631	0.111	85.0	0.7374	0.6269	0.110	85.0
Total System	6.303	0.437	5.274	6.9	6.364	0.432	5.390	6.7

4. Results and discussion:

The ERS has been designed for the input parameters stated in Table 4. The refrigeration capacity is kept fixed at 10 kW. Water is taken as external fluid in generator, condenser and evaporator. The model yielded values of the properties at all states points and mass flow rates of refrigerant and external fluids. These values are presented in Table 5. The COP and entrainment ratio obtained are 0.273 and 0.274 for R1234ze and 0.246 and 0.219 for R134a respectively at the designed conditions.

Table 6 shows exergy loss and exergetic efficiency of the system at the designed conditions. Here the exergy has been obtained using the conventional Gouy-Stodola method. The total exergy of the fuel is the exergy provided to generator and pump, and total exergy of the product is the exergy of evaporator.

Accordingly, the exergy destruction and the exergetic efficiency of the system at the designed conditions for R1234ze are 11.14 kW and 1.4, while for R134a are 12.24 kW and 1.2 respectively. Table 6 shows that more than half of the total exergy loss takes place in ejector followed by generator, condenser, evaporator, pump and throttling valve. Evaporator, throttling valve and pump have very little exergy destruction; together these have 5.7% and 5.8% of the total exergy destruction with R1234ze and R134a respectively. Obviously, the exergetic efficiency of ejector is the lowest among all other components. It is 18.8% and 17.3% for R1234ze and R134a respectively.

Table 4. Input values at design conditions:

Parameters	Values
Generator temperature (T_{Gen} in °C)	95
Condenser temperature (T_{Con} in °C)	36
Evaporator temperature (T_{Eva} in °C)	10
Inlet temperature of external fluid in generator (T_8 in °C)	110
Outlet temperature of external fluid in generator (T_7 in °C)	105

Inlet temperature of external fluid in condenser (T_9 in °C)	27
Outlet temperature of external fluid in condenser (T_{10} in °C)	32
Inlet temperature of external fluid in evaporator (T_{12} in °C)	23
Outlet temperature of external fluid in evaporator (T_{11} in °C)	18
Nozzle efficiency (η_n in %) [44]	90
Diffuser efficiency (η_d in %) [44]	90
Mixing efficiency (η_m in %) [44]	90
Pump efficiency (η_{Pump} in %)	75
Ambient temperature (T_0 in °C)	25
Ambient pressure (P_0 in kPa)	101.32
Refrigeration Capacity (Q_{Eva} in kW)	10

Table 5. Mass flow rate and the Properties at state points:

State Point	T (°C)	P (kPa)		ṁ (refrigerant) (kg/s)		ṁ (water) (kg/s)		h (kJ/kg)		s (kJ/kg/K)	
		R1234ze	R134a	R1234ze	R134a	R1234ze	R134a	R1234ze	R134a	R1234ze	R134a
1	95	2740	3594	0.259	0.296	-	-	427.6	272.3	1.669	0.853
2	47.21	687.4	912.4	0.329	0.358	-	-	419.7	269.3	1.719	0.916
3	36	687.4	912.4	0.329	0.358	-	-	248.5	102.3	1.170	0.376
4	37.66	2740	3594	0.259	0.296	-	-	252.3	105.4	1.172	0.378
5	10	310.3	414.9	0.070	0.065	-	-	248.5	102.3	1.177	0.383
6	10	310.3	414.9	0.070	0.065	-	-	391.0	256.2	1.675	0.926
7	105	143.2	143.2	-	-	2.146	2.338	440.2	440.2	1.363	1.363
8	110	143.2	143.2	-	-	2.146	2.338	461.3	461.3	1.419	1.419
9	27	101.3	101.3	-	-	2.678	2.886	113.1	113.1	0.394	0.394
10	32	101.3	101.3	-	-	2.678	2.886	134.0	134.0	0.464	0.464
11	18	101.3	101.3	-	-	0.478	0.478	75.47	75.47	0.267	0.267
12	23	101.3	101.3	-	-	0.478	0.478	96.39	96.39	0.338	0.338

Table 6: Exergy destruction at the designed input conditions:

Component	$\dot{E}_{F,k}$ (kW)		$\dot{E}_{P,k}$ (kW)		$\dot{E}_{D,k}$ (kW)		ε (%)	
	R1234ze	R134a	R1234ze	R134a	R1234ze	R134a	R1234ze	R134a
Generator	9.896	10.11	7.063	7.1	2.832	3.01	71.4	70.2
Condenser	2.093	2.061	0.862	0.882	1.23	1.179	41.2	42.6
Evaporator	0.518	0.524	0.148	0.08	0.370	0.444	28.6	25.15
Ejector	5.891	6.061	1.108	1.053	4.783	5.008	18.8	17.4
Pump	0.627	0.85	0.470	0.64	0.156	0.21	75.0	75
Throttling valve	0.684	0.684	0.544	0.55	0.139	0.134	79.5	79.9
Total system	10.52	10.96	0.148	0.09	9.51	10.87	1.4	0.8

Table 7**:** Effective temperature and exergy destruction comparison*:*

Component	T_{eff} (K)		$\dot{E}_{D,k}$ (kW) (Gouy-Stodola)		$\dot{E}_{D,k}$ (kW) (Modified Gouy-Stodola)		Difference in $\dot{E}_{D,k}$ (kW)	
	R1234ze	R134a	R1234ze	R134a	R1234ze	R134a	R1234ze	R134a
Generator	380.7	380.7	3.166	3.575	4.045	4.568	27.7	27.7
Condenser	302.5	302.5	1.293	1.319	1.312	1.339	1.5	1.5
Evaporator	293.6	295.6	0.358	0.364	0.353	0.358	-1.4	-1.6
Ejector	320.21	309	4.78	5.413	5.136	5.613	7.4	3.7
Pump	310.66	311.24	0.151	0.217	0.157	0.226	3.9	4.2
Throttling valve	283	283	0.139	0.137	0.133	0.13	-4.3	-5.1
Total system			9.88	11.03	11.14	12.24	12.7	10.9

Table 7 provides effective temperature and also compares exergy destruction obtained by the conventional and modified Gouy-Stodola equations at the designed input conditions. Both the methods confirm that the ejector has the highest exergy destruction, though the values obtained by the modified approach are higher. In the conventional approach, irreversibility loss in the evaporator and throttling valve is more as compared to the new equation, as their effective temperatures are lower as compared to the surrounding temperature. The total irreversibility rate in ERS calculated by modified analysis is 11.14 kW and 12.24 kW for R1234ze and R134a respectively. It is 12.7% higher with R1234ze and 10.9% higher with R134a when calculated by the conventional equation. This study clearly reveals the difference between the two approaches of exergy analysis.

4.1 Performance parameters and area ratio with the generator temperature:

Fig. 3 highlights the impact of varying the generator temperature on performance parameters i.e. COP, Entrainment Ratio (μ) and area ratio (AR). The other input conditions are kept same as the designed conditions stated in table 4. Figure 3 shows that there is enhancement in COP, μ and area ratio with the rise in generator temperature.

The rise in generator temperature drops the requirement of primary/motive flow rate. However, the secondary mass flow rate remains constant for the fixed cooling capacity and other inputs parameters. It increases μ and COP. The AR of ejector extends to accommodate the high-pressure primary fluid expansion up to the same back pressure. The AR at designed conditions is 5.971 for R1234ze and 5.761 for R134a and it changes to 6.568 for R1234ze and 6.26 for R134a at 99°C generator temperature. The COP and μ are increased by 15.9% and 14.7% respectively for R1234ze with the change in generator temperature from 91°C to 99°C and for the same temperature range; COP and μ for R134a are increased by 12.9% and 8.1% respectively.

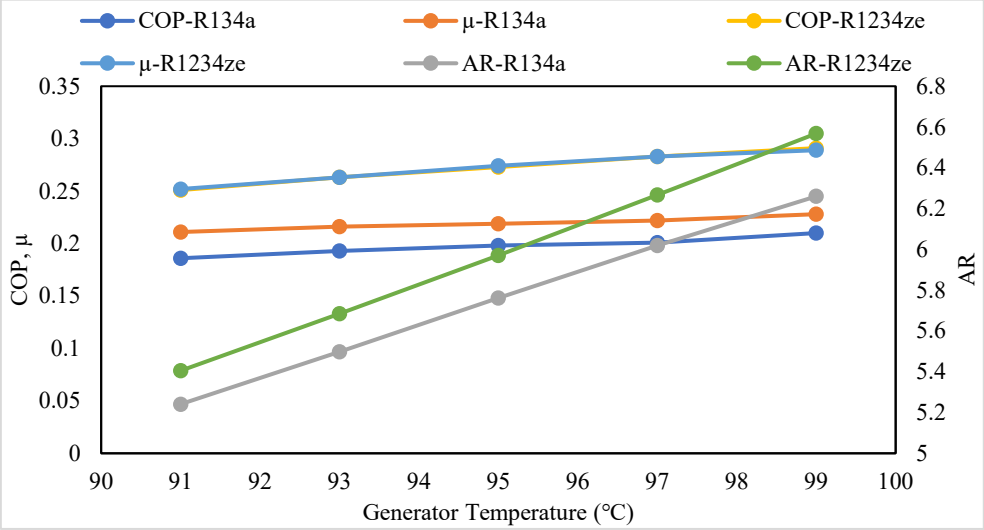

Fig. 3: COP, μ and AR with the generator temperature

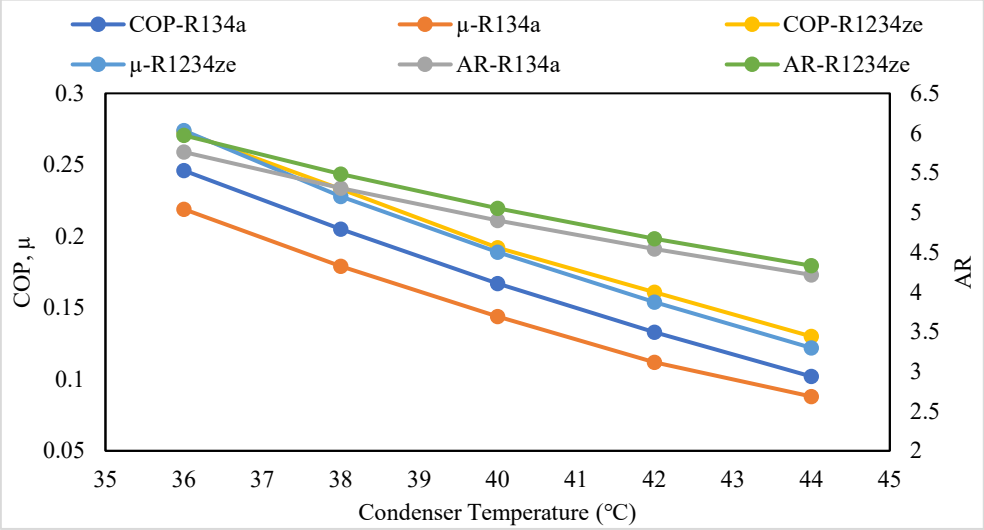

Fig. 4: COP, μ and AR with the condenser temperature

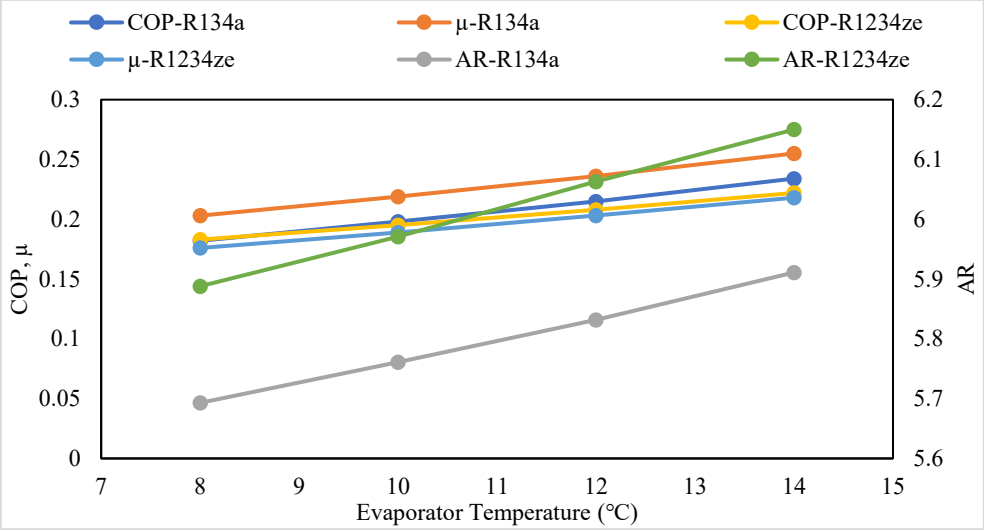

Fig. 5: COP, μ and AR with the evaporator temperature

4.2 Performance parameters and area ratio with the condenser temperature:

Fig. 4 depicts the effect of condenser temperature on COP, μ and AR. The other input conditions are kept same as mentioned in table 4. The graph shows that COP, μ and AR are decreased as the condenser temperature is increased. The rise in condenser temperature raises both the primary and secondary fluid mass flow rate. However, the increase in primary mass flow rate is more than the secondary mass flow rate, thus μ is decreased, hence COP.

The AR of the ejector gets reduced to attain more velocity of mixing that is utilized to meet high-pressure condenser requirements. At 40°C, the area ratio is 5.053 for R1234ze and 4.9 for R134a. The COP and μ are found to decrease by 52.4% and 55.5% for R1234ze; and 61.6% and 59.8% for R134a, respectively, with the rise in condenser temperature from 36°C to 44°C.

4.3 Performance parameters and area ratio with the evaporator temperature:

Fig. 5 shows that COP, μ, and AR are increased with the evaporator temperature. Increasing the evaporator temperature lowers the primary and secondary fluid mass flow rates. However, the decrease in primary mass flow rate is more than the secondary mass flow rate, thus, μ is increased, hence COP. The AR of ejector is found to decrease with the rise in evaporator temperature. At 14°C, the area ratio is 6.1 for R1234ze and 5.9 for R134a. The COP and μ are increased by 21.3% and 23.8% for R1234ze; and 28.6% and 25.6% for R134a respectively, with the change in evaporator temperature from 8°C to 14°C.

4.4 Irreversibility in the generator with its temperature:

Fig. 6 illustrates the variation of irreversibility and

exergetic efficiency of generator with respect to its own temperature. Other input parameters are same as shown in table 4. The figure shows that the irreversibility of the generator is decreased; therefore, exergetic efficiency is enhanced with the rise in generator temperature. The trend of irreversibility variation is same with both the equations, but the irreversibility calculated by the conventional method is 21.7% under estimated than the modified method for R1234ze.

Increasing generator temperature lowered entropy generation because of the drop in the flow rate of primary and external fluids. At 91°C, the irreversibility obtained by the conventional and the modified Gouy-Stodola equations are 3.67 kW and 4.69 kW respectively for R1234ze; and 4.01 kW and 5.54 kW respectively for R134a. At the designed conditions, these values are 3.16 kW and 4.04 kW respectively for R1234ze; and 3.57 kW and 4.56 kW respectively for R134a. The exergy of product and fuel is found to decrease due to the drop in flow rate of primary and external fluids with the increase in generator temperature. It increased the exergetic efficiency. The exergetic efficiency is increased by 3.5% for R134a and 5.6% for R1234ze with the change in generator temperature from 91°C to 99°C.

4.5 Irreversibility in the condenser with its temperature:

Fig. 7 illustrates the trend of irreversibility and exergetic efficiency of the condenser with respect to its temperature. The figure shows that the irreversibility is increased, and so exergetic efficiency is reduced if the condenser temperature is increased. The trend of irreversibility variation is same with both the equations, and there is not a big difference in the values as well. Increasing condenser temperature enhanced the entropy generation due to the increase in mass flow rates of mixed fluid and external fluid. The irreversibility calculated by the modified method is only 1.5% higher than the conventional method for both the refrigerants R134a and R1234ze. The maximum exergetic efficiency is 0.4% for R134a and 0.4% for R1234ze at 36°C condenser temperature.

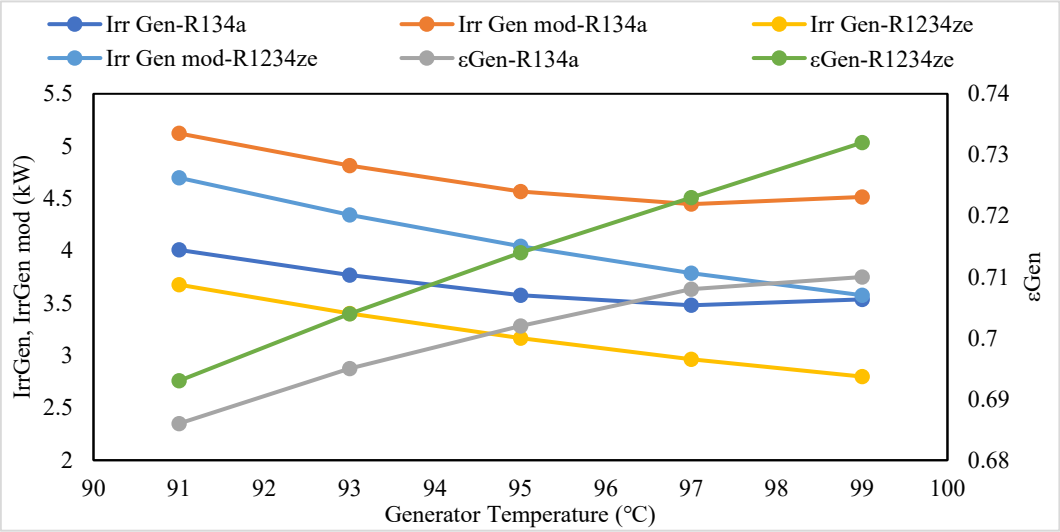

Fig. 6: Irreversibility in the generator with its temperature

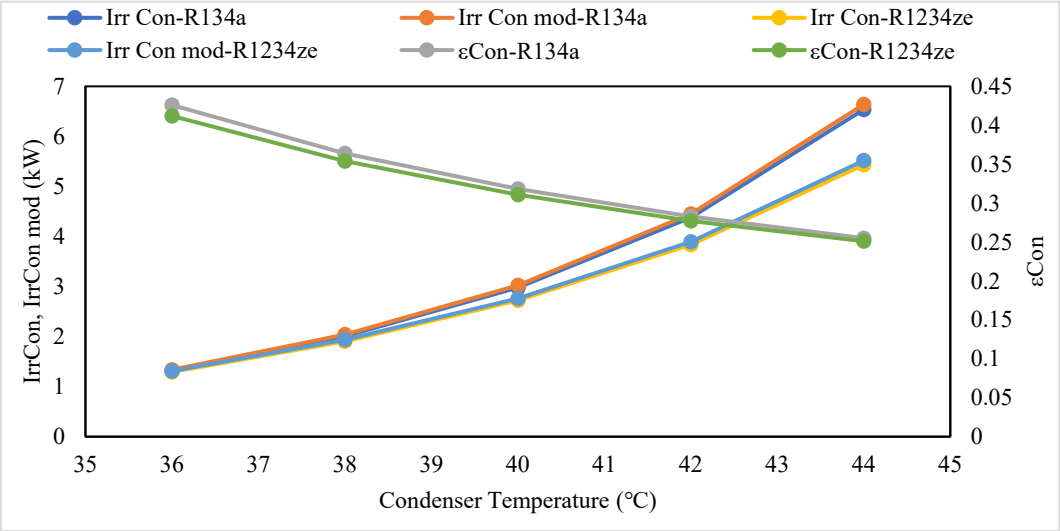

Fig. 7: Irreversibility in the condenser with its temperature

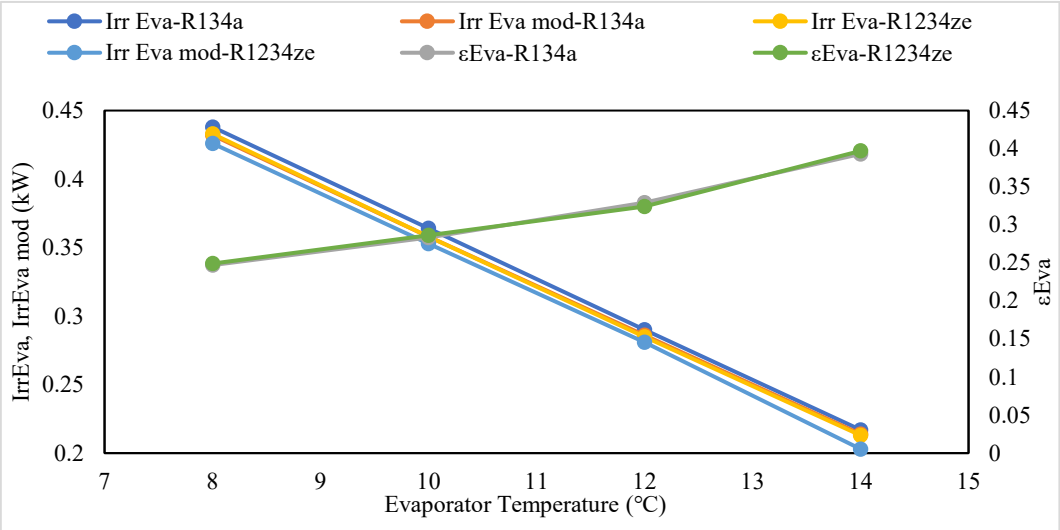

Fig. 8: Irreversibility in the evaporator with its temperature

4.6 Irreversibility in the evaporator with its temperature:

Fig. 8 presents the variation of irreversibility loss and the exergetic efficiency of evaporator with its temperature. The figure shows that the irreversibility is decreased, and thus exergetic efficiency is improved with the rise in evaporator temperature. Enhancing evaporator temperature decreases the exergy of fuel, as the secondary fluid flow rate decreases, but the exergy of the product remains constant due to constant external fluid mass flow rate; thus exergetic efficiency is increased. Increasing evaporator temperature decreased the entropy generation reason being the decrease in secondary fluid mass flow rate and so the irreversibility. The irreversibility calculated by the modified method is 1.65% and 1.4% underestimated for R134a and R1234ze respectively than the conventional method. The exergetic efficiency is increased by 59.1% for R134a and 59.4% for R1234ze respectively with the rise in generator temperature from 8°C to 14°C.

4.7 Irreversibility in the ejector with the generator temperature:

Fig. 9 provides the variation of irreversibility loss in ejector with the generator temperature keeping other parameters constant as shown in table 4. It shows that the increase in generator temperature lowers the irreversibility of ejector.

Raising the generator temperature decreased entropy of the mixed fluid and that of the primary fluid while the entropy of the secondary fluid remained constant. It lowered the entropy generation of ejector and hence irreversibility rate. At designed conditions, i.e. 95°C

generator temperature, the values of I_{Eje}, $I_{Eje,m}$ are 4.78 kW and 5.14 kW respectively for R1234ze; and 5.413 kW and 5.613 kW respectively for R134a. The irreversibility calculated by conventional and modified methods is decreased by 4.6% and 4.9% respectively for R1234ze and 5.4% and 5.5% respectively for R134a with the change in generator temperature from 91°C to 99°C.

4.8 Irreversibility in the ejector with the condenser temperature:

Fig. 10 presents the outcome of condenser temperature variation on the irreversibility of ejector, keeping all other parameters constant. It shows that the increase in condenser temperature enhances the irreversibility of ejector.

Increasing the condenser temperature is found to increase the entropy of mixed, primary and secondary fluids due to the rise in their mass flow rates. The effective temperature is also increased; therefore, entropy generation of the ejector is increased, and thus the irreversibility rate. At designed conditions, irreversibility determined by the modified method is 7.5% and 3.7% more than that determined by the traditional method for R1234ze and R134a respectively.

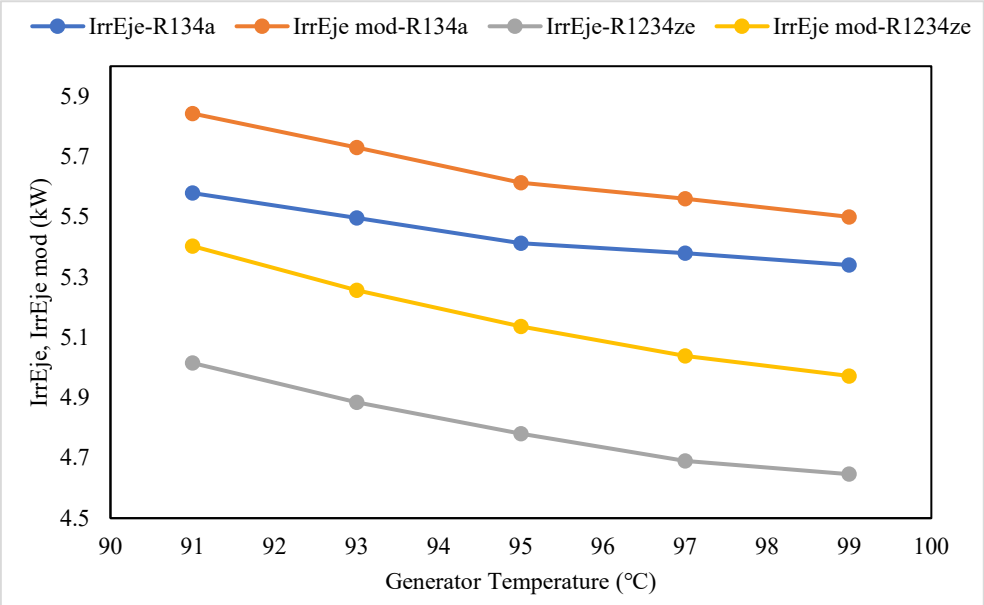

Fig.9: Irreversibility in the ejector with the generator temperature

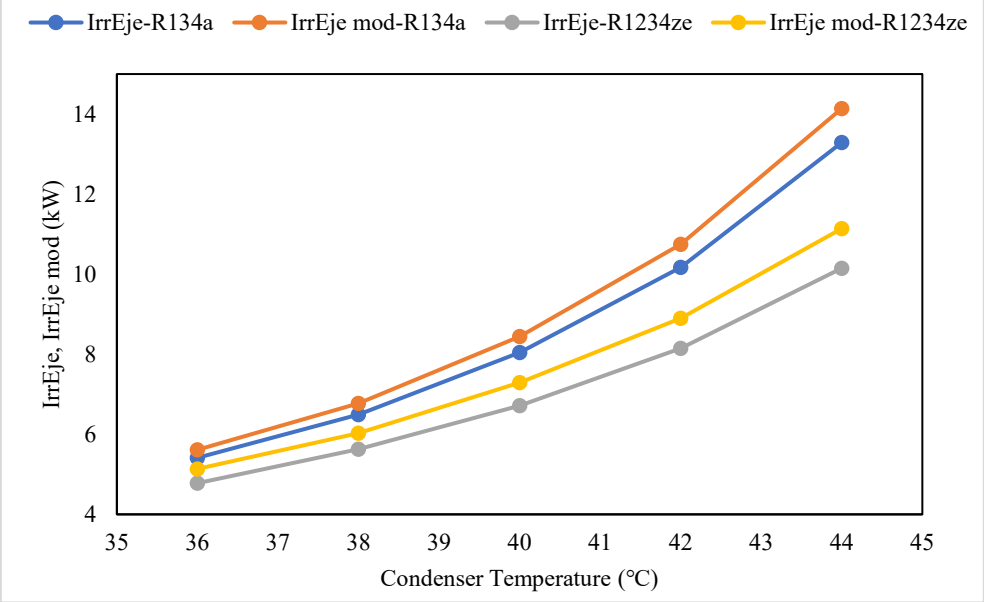

Fig.10: Irreversibility in the ejector with the condenser temperature

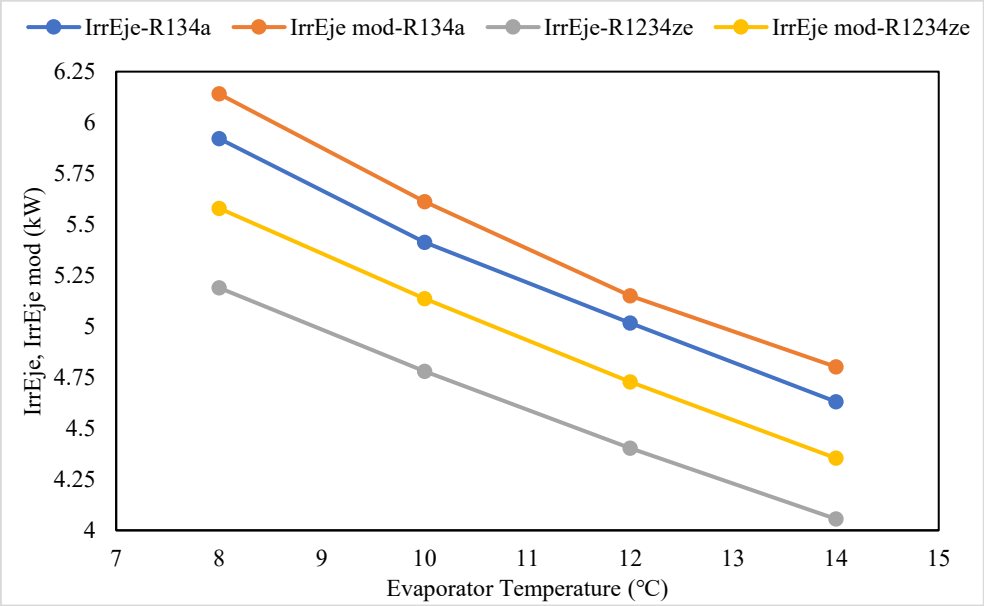

Fig.11: Irreversibility in the ejector with the evaporator temperature

4.9 Irreversibility in the ejector with the evaporator temperature:

Fig. 11 shows that rise in evaporator temperature reduces the irreversibility loss in ejector. The entropy of mixed fluid and of primary and secondary fluids is decreased and also the effective temperature; therefore, the irreversibility rate is decreased. The irreversibility determined by the modified approach is found to be 7.4% and 3.7% higher for R134a and R1234ze respectively than the conventional approach when the evaporator temperature is raised from 8°C to 14°C. At the designed conditions, the ejector irreversibility determined by the conventional and modified equations are 4.78kW and 5.14kW respectively for R1234ze; and 5.413kW and 5.613kW respectively for R134a.

4.10 CSB of the generator:

Fig. 12 shows that the total irreversibility calculated by the modified method and the irreversibility of generator itself is decreased with the increase in generator temperature. Moreover, the slopes of the curves indicate that the change in total irreversibility is 1.56 and 1.54 times higher than the change in irreversibility of the generator due to its temperature for R1234ze and R134a respectively. The higher the value of slope i.e. CSB means higher the sensitivity of system due to the change in the parameter considered.

4.11 CSB of the condenser:

Fig. 13 depicts that total irreversibility and irreversibility of condenser itself are increased with the increase in condenser temperature. The CSB is 4.14 and 4.26 with the condenser temperature change for R1234ze and R134a respectively. The total irreversibility of system and condenser are increased by 168.3% and 326.7% respectively for R1234ze with the change in condenser temperature from 36°C to 44°C.

4.12 CSB of the evaporator:

Fig. 14 shows that the total irreversibility and the irreversibility of evaporator are decreased with the rise in evaporator temperature. The CSB is 15.59 and 20.51 with the evaporator temperature change for R1234ze and R134a respectively. It means that a little change in the temperature of evaporator makes the system more irreversible in comparison to the same change in the temperatures of condenser or generator. The total irreversibility of system and evaporator is decreased by 23.5% and 50.9% respectively for R1234ze with the variation of evaporator temperature from 8°C to 14°C.

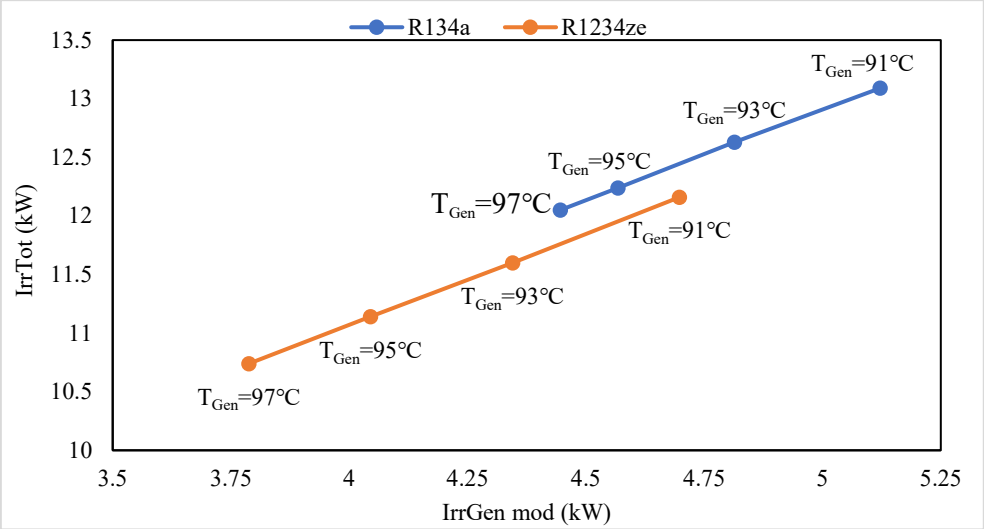

Fig.12: Total irreversibility with the generator temperature

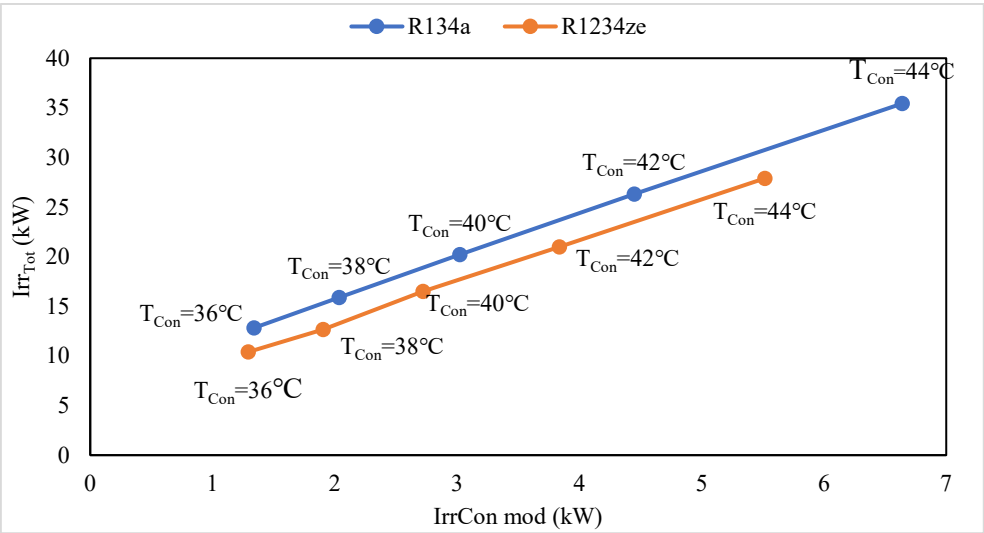

Fig.13: Total irreversibility with the condenser temperature

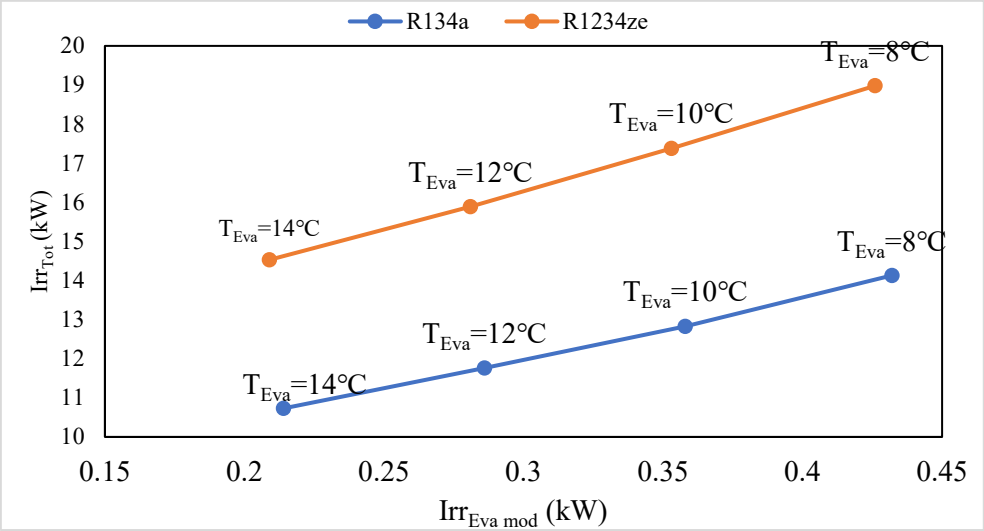

Fig.14: Total irreversibility with the evaporator temperature

5. Conclusions:

This paper presents the exergy analysis of ERS for a relatively new ecofriendly refrigerant R1234ze using the modified Gouy-Stodola formulation. The theory of effective temperature has been applied to calculate the irreversibility rate of the system components.

- Total exergy loss calculated by the conventional Guoy-Stodola equation is 10.4 kW, whereas it is 11.62 kW by the modified Gouy-Stodola equation for R1234ze as working fluid, whereas these values are 11.65 kW and 12.83kW respectively for R134a.
- The ejector has the highest irreversibility, followed by generator, condenser, evaporator, pump and throttling valve.
- The COP is increased by 15.93% for R1234ze with the change in generator temperature from 91°C to 99°C and for the same temperature range, COP is increased by 12.9% for R134a. The COP is decreased by 52.4% for R1234ze but 61.6% for R134a with the rise in condenser temperature from 32°C to 40°C. It is concluded that R1234ze performs better than R134a.
- The CSB values for generator, condenser and evaporator are 1.62, 4.14, and 15.59 respectively for R1234ze and 1.64, 4.26 and 20.5 respectively for R134a. The evaporator is found to be more sensitive to changes in its temperature due to the highest CSB value.

Nomenclature

AR	Area ratio (-)
COP	coefficient of performance (–)
CSB	Coefficient of structural bonds (-)
ERS	Ejector refrigeration system (-)
GWP	Global warming potential (-)
ODP	Ozone depletion potential (-)
Ma	Mach Number (-)
VCRS	Vapor compression refrigeration system (-)

Greek symbols

μ	Entrainment ratio (-)
ε	Exergetic efficiency (%)

Subscripts

Con	Condenser
D	Destruction
eff	Effective
Eje	Ejector
Eva	Evaporator
F	Fuel
Gen	Generator
gen	generation
in	Inlet state
m	Mixing
max	Maximum
mod	Modified
n	Nozzle
out	Outlet state
P	Product
Pump	Pump
r	Reversible process
TV	Throttling Valve
tot	Total
1,2,3..	State points
e_1, e_2, e_3....	State points inside the ejector
0	Ambient condition

References

1) B.J. H Keenan, E.P. Neumann, and F. Lustwerk, "An Investigation of Ejector Design by Analysis and Experiment," 1950. http://asmedigitalcollection.asme.org/appliedmechanics/article-pdf/17/3/299/6746651/299_1.pdf.
2) B.J. Huang, J.M. Chang, C.P. Wang, and V.A. Petrenko, "A 1-d analysis of ejector performance," *International Journal of Refrigeration*, **22** (*5*) 354–364 (1999). doi:10.1016/S0140-7007(99)00004-3.
3) A. Selvaraju, and A. Mani, "Experimental investigation on r134a vapour ejector refrigeration system," *International Journal of Refrigeration*, **29** (*7*) 1160–1166 (2006). doi:10.1016/J.IJREFRIG.2006.01.004.
4) T. Sankarlal, and A. Mani, "Experimental investigations on ejector refrigeration system with ammonia," *Renew Energy*, **32** (*8*) 1403–1413 (2007). doi:10.1016/J.RENENE.2006.05.008.
5) J. Chen, H. Havtun, and B. Palm, "Investigation of ejectors in refrigeration system: optimum performance evaluation and ejector area ratios perspectives," *Appl Therm Eng*, **64** (*1–2*) 182–191 (2014). doi:10.1016/J.APPLTHERMALENG.2013.12.034.
6) M. Purjam, K. Thu, and T. Miyazaki, "Thermodynamic feasibility evaluation of a novel low-temperature ejector-based trans-critical r744 refrigeration cycle," *Evergreen*, **8** (*1*) 204–212 (2021). doi:10.5109/4372280.
7) J. Yan, G. Chen, C. Liu, L. Tang, and Q. Chen, "Experimental investigations on a r134a ejector applied in a refrigeration system," *Appl Therm Eng*, **110** 1061–1065 (2017). doi:10.1016/J.APPLTHERMALENG.2016.09.046.
8) V. Kumar, and G. Sachdeva, "Experimental

investigation of ejector-assisted vapor compression system," *International Journal of Air-Conditioning and Refrigeration*, **27** (*3*) (2019). doi:10.1142/S2010132519500299.

9) V. Kumar, and G. Sachdeva, "1-d model for finding geometry of a single phase ejector," *Energy*, **165** 75–92 (2018). doi:10.1016/J.ENERGY.2018.09.071.
10) X. Ma, W. Zhang, S.A. Omer, and S.B. Riffat, "Experimental investigation of a novel steam ejector refrigerator suitable for solar energy applications," *Appl Therm Eng*, **30** (*11–12*) 1320–1325 (2010). doi:10.1016/j.applthermaleng.2010.02.011.
11) R. Yapici, "Experimental investigation of performance of vapor ejector refrigeration system using refrigerant r123," *Energy Convers Manag*, **49** (*5*) 953–961 (2008). doi:10.1016/J.ENCONMAN.2007.10.006.
12) N. Bilir Sag, and H.K. Ersoy, "Experimental investigation on motive nozzle throat diameter for an ejector expansion refrigeration system," *Energy Convers Manag*, **124** 1–12 (2016). doi:10.1016/j.enconman.2016.07.003.
13) B. Kitrattana, S. Aphornratana, and T. Thongtip, "One dimensional steam ejector model based on real fluid property," *Thermal Science and Engineering Progress*, **25** (2021). doi:10.1016/j.tsep.2021.101016.
14) B. Sharma, S. Shubham, and G. Sachdeva, "Performance prediction of ejector refrigeration system using R1234yf as working fluid," in: J Phys Conf Ser, Institute of Physics Publishing, 2019. doi:10.1088/1742-6596/1240/1/012128.
15) G.A. Untea, A. Dobrovicescu, L. Grosu, and E.C. Mladin, "ENERGY and exergy analysis of an ejector refrigeration system," *U.P.B. Sci. Bull., Series D*, **75** (2013).
16) A. Baruah, D.K. Saini, and G. Sachdeva, "Exergy investigation of a vapor compression system comprising ejector for isentropic expansion," in: J Phys Conf Ser, Institute of Physics Publishing, 2019. doi:10.1088/1742-6596/1240/1/012125.
17) W. Pridasawas, and P. Lundqvist, "An exergy analysis of a solar-driven ejector refrigeration system," *Solar Energy*, **76** (*4*) 369–379 (2004). doi:10.1016/J.SOLENER.2003.11.004.
18) G.K. Alexis, "Exergy analysis of ejector-refrigeration cycle using water as working fluid," *Int J Energy Res*, **29** (*2*) 95–105 (2005). doi:10.1002/er.1042.
19) A. Dahmani, Z. Aidoun, and N. Galanis, "Optimum design of ejector refrigeration systems with environmentally benign fluids," *International Journal of Thermal Sciences*, **50** (*8*) 1562–1572 (2011). doi:10.1016/J.IJTHERMALSCI.2011.02.021
20) J. Chen, H. Havtun, and B. Palm, "Conventional and advanced exergy analysis of an ejector refrigeration system," *Appl Energy*, **144** 139–151 (2015). doi:10.1016/j.apenergy.2015.01.139.
21) J. Chen, K. Zhu, Y. Huang, Y. Chen, and X. Luo, "Evaluation of the ejector refrigeration system with environmentally friendly working fluids from energy, conventional exergy and advanced exergy perspectives," *Energy Convers Manag*, **148** 1208–1224 (2017). doi:10.1016/j.enconman.2017.06.051.
22) M.Q. Zeng, Q.Y. Zheng, X.L. Zhang, F.Y. Mo, and X.R. Zhang, "Thermodynamic analysis of a novel multi-target temperature transcritical co2 ejector-expansion refrigeration cycle with vapor-injection," *Energy*, **259** 125016 (2022). doi:10.1016/J.ENERGY.2022.125016.
23) T. Bai, R. Shi, and J. Yu, "Thermodynamic performance evaluation of an ejector-enhanced transcritical co2 parallel compression refrigeration cycle," *International Journal of Refrigeration*, (2022). doi:10.1016/J.IJREFRIG.2022.12.014.
24) J. qiang Deng, P. xue Jiang, T. Lu, and W. Lu, "Particular characteristics of transcritical co2 refrigeration cycle with an ejector," *Appl Therm Eng*, **27** (*2–3*) 381–388 (2007). doi:10.1016/J.APPLTHERMALENG.2006.07.016.
25) M. Yari, "Performance analysis and optimization of a new two-stage ejector-expansion transcritical co2 refrigeration cycle," *International Journal of Thermal Sciences*, **48** (*10*) 1997–2005 (2009). doi:10.1016/j.ijthermalsci.2009.01.013.
26) X. Liu, K. Yu, X. Wan, M. Zheng, and X. Li, "Conventional and advanced exergy analyses of transcritical co2 ejector refrigeration system equipped with thermoelectric subcooler," *Energy Reports*, **7** 1765–1779 (2021). doi:10.1016/J.EGYR.2021.03.023.
27) D. Li, and E.A. Groll, "Transcritical co2 refrigeration cycle with ejector-expansion device," *International Journal of Refrigeration*, **28** (*5*) 766–773 (2005). doi:10.1016/j.ijrefrig.2004.10.008.
28) Gao. Yu, He Guogeng, Cai Dehua and Fan Mingjing, "Performance evaluation of a modified R290 dual-evaporator refrigeration cycle using two-phase ejector as expansion device" Energy **212** (2020) 118614, https://doi.org/10.1016/j.energy.2020.118614.
29) Kornhauser AA, Menegay P. Method of reducing flow metastability in an ejector nozzle. US Patent no. 5343711; 1994
30) Menegay P, Kornhauser AA. Improvement to the ejector expansion refrigeration cycle. In: Proceedings of the intersociety energy conversion engineering conference, vol. 2, Washington DC; 1996. p.702–6.
31) J.G. Speight, "A review of: 'the exergy method: technical and ecological applications,'" *Energy Sources*, **27** (*11*) 1099–1101 (2005). doi:10.1080/00908310500214958.
32) H. Holmberg, P. Ruohonen, and P. Ahtila, "Determination of the real loss of power for a condensing and a backpressure turbine by means of second law analysis," *Entropy*, **11** (*4*) 702–712 (2009).

doi:10.3390/e11040702.
33) M.J. Lampinen, and R. Wikstén, "Theory of effective heat-absorbing and heat-emitting temperatures in entropy and exergy analysis with applications to flow systems and combustion processes," *Journal of Non-Equilibrium Thermodynamics*, **31** (*3*) 257–291 (2006). doi:10.1515/JNETDY.2006.012.
34) U. Perera, N. Takata, T. Miyazaki, Y. Higashi, and K. Thu, "The exergy investigation of a mechanical vapor compression chiller for cooling using r410a," *Evergreen*, **8** (*1*) 213–220 (2021). doi:10.5109/4372281.
35) V. Jain, G. Sachdeva, and S.S. Kachhwaha, "Thermodynamic modelling and parametric study of a low temperature vapour compression-absorption system based on modified gouy-stodola equation," *Energy*, **79** (*C*) 407–418 (2015). doi:10.1016/J.ENERGY.2014.11.027.
36) V. Jain, S. Singh Kachhwaha, and G. Sachdeva, "Exergy analysis of a vapour compression-absorption cascaded refrigeration system using modified Gouy-Stodola equation," 2014.
37) G. Sachdeva, and B. Sharma, "Exergy analysis of an ejector cooling system by modified gouy-stodola equation," *International Journal of Air-Conditioning and Refrigeration*, **29** (*3*) (2021). doi:10.1142/S2010132521500279.
38) B. Sharma, G. Sachdeva, and V. Kumar, "Exergy analysis of heat assisted ejector refrigeration system using r1234yf," *IOP Conf Ser Mater Sci Eng*, **1104** (*1*) 012035 (2021). doi:10.1088/1757-899x/1104/1/012035.
39) C. Nikolaidis, and D. Probert, "Exergy-method analysis of a two-stage vapour-compression refrigeration-plants performance," n.d.
40) B.H. Gebreslassie, M. Medrano, F. Mendes, and D. Boer, "Optimum heat exchanger area estimation using coefficients of structural bonds: application to an absorption chiller," *International Journal of Refrigeration*, **33** (*3*) 529–537 (2010). doi:10.1016/j.ijrefrig.2009.12.004.
41) J. Yu, Y. Ren, H. Chen, and Y. Li, "Applying mechanical subcooling to ejector refrigeration cycle for improving the coefficient of performance," *Energy Convers Manag*, **48** (*4*) 1193–1199 (2007). doi:10.1016/j.enconman.2006.10.009.
42) H. El-Dessouky, H. Ettouney, I. Alatiqi, and G. Al-Nuwaibit, "Evaluation of steam jet ejectors," 2002. www.elsevier.com/locate/cep.
43) D.-W. Sun, "Performance Characteristics Of Hcfc-123 Ejector Refrigeration Cycles," 1996.
44) B. Saleh, "Performance analysis and working fluid selection for ejector refrigeration cycle," *Appl Therm Eng*, **107** 114–124 (2016). doi:10.1016/j.applthermaleng.2016.06.147.
45) Nacak Cihan and Sarac Betul, "The performance assessment of a refrigeration system which exists on a cargo vessel influenced by seawater-intake temperature" Journal of Thermal Analysis and Calorimetry (2021) 146:1229–1243 https://doi.org/10.1007/s10973-020-10060-y.
46) Engineering equation solver, academic professional license 4278, national institute of technology, Kurukshetra, India.